Innovative: International Multi-disciplinary Journal of Applied Technology
(ISSN 2995-486X) VOLUME 02 ISSUE 11, 2024

A Silica Core-Shell Cylinder Photonic Nanojet with Cylindrical Pores

Shakhawan Jalal Jabar, Sardar Mohamed Law Sleman, Mohammed Arif Othman
THE Ministry of Education

Abstract:

A tunable photonic nanojet structure is proposed based on a silica core-shell microcylinder with cylindrical pores. The exact solution of electromagnetic wave scattering from silica core-shell microcylinder was done using the boundary value problem. The effects of porosity, core diameter, shell thicknesses, and type of incident light polarization on the main parameters of photonic nanojet were studied. The results show that with the porosity increasing the photonic nanojet length, focal length, and full with at half maximum of photonic nanojet are increased. However, energy enhancement in the focal spot is decreased by increasing porosity. Furthermore, in many structural conditions, the focal length for TE polarized light is larger or equal to the TM polarization case. The proper photonic nanojet for particular applications is accessible by tuning the geometrical and physical parameters of the porous silica core-shell microcylinder.

Keywords: Photonic Nanojet, Porosity, Porous Silica, Scattering, Microcylinder.

Introduction

The photonic nanojet (PNJ) is produced when a dielectric microcylinder or microsphere is illuminated with light radiation. Redistribution and localized confinement of incident electromagnetic wave energy on the shadow side of the dielectric object led to the formation of a PNJ. The energy enhancement and localization properties of photonic nano-jet as well as its narrow waist and long length have made it a powerful instrument for applications in a wide range of optical technologies such as two-photon fluorescence enhancement [1], optical nanoparticle detection and trapping [2-5], high-resolution optical imaging [6], nano-photonic lithography [7,8], Biological cell trapping [9], and optical tweezers[10,11].

Adjusting the refractive index, size, and shape of the scatterer dielectric is a simple method to improve PNJ characteristics. Many experimental and theoretical works have been done in this field [12-17]. These studies show that the characteristics of the PNJ depend on the radius and refractive

index of the microsphere or microcylinder and the wavelength of incident electromagnetic waves. Ferrand et al. [12] using a fast scanning confocal microscope system, reported experimental observation of PNJ produced by single latex microspheres (with refractive index 1.6 and diameters 1-5 μm) illuminated by a 520 nm wavelength plane wave. Kong et al. used the three-dimensional finite difference time domain (FDTD) method to demonstrate that a graded-index dielectric microsphere can generate longer PNJ than a homogeneous microsphere [13]. Soh et al. reported that the full width at half maximum (FWHM) and length of the PNJ can be tuned by varying the temperature of the vanadium oxide which is coated on one side of a glass microsphere and illuminated with incident 800 nm wavelength light [15]. They also optimized the thicknesses of the vanadium oxide coated layer, the microsphere diameter, and its refractive index to achieve the best performance.

Liu et al. investigated the properties of PNJ generated by a two-layer dielectric hemisphere [14]. They have shown that the PNJ produced with the two-layer dielectric hemisphere has superior performance in the jet length and the focal distance compared to that of the homogeneous hemisphere. The authors of reference [16], numerically studied the PNJ produced with biocompatible hydrogel core-shell microspheres with different refractive indexes. They found that the presence of the shell layer can significantly affect the parameters of the PNJ. They claimed that their tunable PNJ produced from the biocompatible hydrogel core-shell microspheres could be useful in future biosensing applications. Yang et al. [17] investigated the generation of PNJ by various metallic-coated dielectric microcylinders through the finite difference time domain method. The intensity of PNJ can be tuned by varying the thickness of the metallic coating layer.

Various incident wave characteristics such as wavefront type and its polarization, have been proposed as another way to manipulate PNJ properties. Yousefi et al. [18] reported the generation of PNJ under converging and diverging beams. The PNJ properties, including the focal length and the full width at half maximum, were studied by changing the source curvature. Li et al. [19] explored the manipulation of PNJ through axial illumination of cylindrical dielectric particles with radially and azimuthally polarized cylindrical vector beams. Chen et al. [20]investigated the effect of polarization and the incident wave amplitude profile on the PNJ properties generated with illuminated dielectric microspheres with light waves. PNJ can be formed suitable for specific applications by designing the polarization and amplitude profile of the incident light. Uenohara et al. [21] have studied controlling the PNJ intensity by adjusting the intensity distribution of two incident Gaussian and radially polarized laser beams. They demonstrated that a large and small PNJ beam diameter could be obtained by a Gaussian and a radially polarized beam, respectively.

Adjusting the porosity of porous material can be the basis for generating materials with tunable optical properties [22,23]. Fabrication of porous materials is possible empirically in three classes: micropores, mesopores, and macropores materials [24]. Microlithography and colloidal self-assembly are different porous material fabrication techniques [25]. Porous silica is an ideal tunable refractive index material. Numerous porous silica substrates can be selected according to the application field. Porous silica production through colloidal crystallization was introduced by Velev et al. [26]. Huang et al. recently prepared porous silica using plant-derived silica sources and self-assembled lignin templates [27]. In this paper, considering the possibility of production material with an adjustable refractive index with a porous material a PNJ with tunable properties in the visible region has been studied using porous silica core-shell microcylinder. The boundary value problem was employed to calculate electromagnetic wave scattering from dielectric microcylinders. The simulation results showed that high-performance PNJ can be achieved by tuning the porosity of silica for optimum value.

Theoretical background

Figure 1 illustrates the PNJ schema generated by a linear polarized plane electromagnetic wave incident on a porous silica core-shell microcylinder. The dielectric microcylinder core (with diameters D=5 and 6 μm) contains cylindrical pores with various porosity (P) from 0 to 0.75. The shell of the cylinder (with thicknesses d= 0.25, 0.50, 0.75, and 1.00 μm) is made of fused silica. The incident electromagnetic wave is TE or TM polarized light with a wavelength λ =

632.8 nm propagating in the x-axis direction.

Focal length f, length of photonic nanojet L, energy enhancement or relative intensity, and full width at half maximum (FWHM) are the four main parameters studied in this research. These characteristics are depicted in Figure 1. The focal length f is measured from the shadow surface of the microcylinder to the point of maximum intensity on the axis of PNJ. The peak intensity of a PNJ is commonly expressed in terms of the relative intensity at the maxima in the axial intensity distribution of the PNJ. Peak intensity denotes the intensity enhancement of the incident field due to the localization of the field in the PNJ beam. The length of a PNJ is defined as the distance from the start point of the PNJ formation until its end. The PNJ waist is denoted by the full width at half maximum (FWHM) of the transverse intensity profile measured at the focal point.

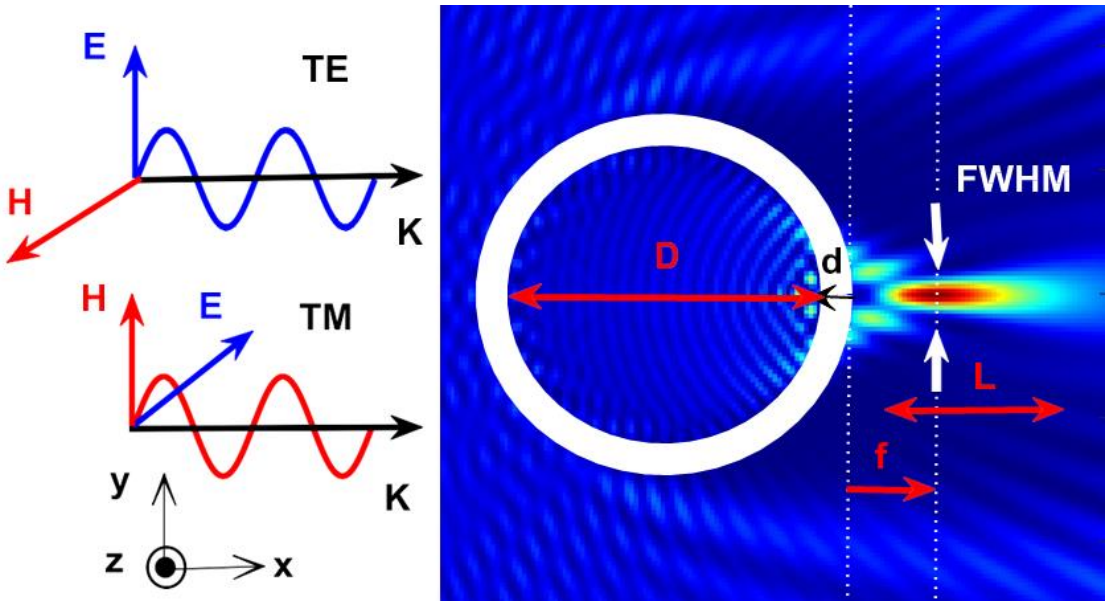

Fig 1. Linear polarized light incidence on silica core-shell cylinder and photonic nanojet characteristics.

The boundary value method [28] is used in this paper to solve the scattering of electromagnetic waves by core-shell dielectric microcylinder. In this method, the continuity of tangential components of the electric and magnetic fields of the electromagnetic waves is considered at the boundaries.

The vector wave equations in a homogeneous medium can be taken as follows for the time dependency of the electromagnetic plane wave as ($E, H \sim exp(-i\omega t)$) [29].

$$A^2\vec{E}\rightarrow + k_j^2\vec{E}\rightarrow = 0$$

$$A^2\vec{H}\rightarrow + k^2\vec{H}\rightarrow = 0 \quad (1)$$

Where, E and H are the electric and magnetic field components of electromagnetic waves, respectively, and $k_j = \frac{2\pi\sqrt{\varepsilon_j}}{\lambda}$ is the wave number in each region. Here there are three regions:

surrounding medium (air), shell (fused silica), and core (porous silica). The electric permittivity of air and fused silica at the wavelength 632.8 nm are 1 and 2.123 [30], respectively. The effective permittivity of porous silica must be considered for the core of the dielectric microcylinder. Brandt et al. [22] described the optical properties of dielectric materials with cylindrical pores via Maxwell Garnett [31] and the Bruggeman [32] effective medium models. Their experimental results with macroporous and mesoporous silicon agree very well with the Maxwell-Garnett model. So, in this study, we employed the Maxwell-Garnett model to calculate the effective permittivity of porous silica. The effective permittivity of air-silica composite with the porosity percentage filling by air (P) can be written as [33]:

$$\varepsilon_{eff} = \frac{A_a P s_a + A_s (1-P) s_s}{A_a P + A_s (1-P)} \qquad (2)$$

Where ε_a and ε_s are the electric permittivity of air and fused silica, respectively. In the TM polarized (electric field along cylinder axis) case the field enhancement factors are equal to one ($A_a = A_s = 1$) [34]. So, equation (2) becomes as follows for TM polarization.

$$\varepsilon_{eff,TM} = P\varepsilon_a + (1-P)\varepsilon_s \qquad (3)$$

In the case of the electric field perpendicular to the cylinder axis (TE polarization), the field enhancement factors are $A_a = 2\varepsilon_s/(\varepsilon_a + \varepsilon_s)$ and $A_s = 1$ [34]. The effective electric permittivity for this polarization is denoted by equation (4).

$$\varepsilon_{eff,TE} = \varepsilon_s \frac{(1-P)s_s + (1+P)s_a}{(1+P)s_s + (1-P)s_a} \qquad (4)$$

The reference [28] method was employed to solve equations (1). Matching conditions at each boundary surface were applied. The electric and magnetic field components of electromagnetic waves are obtained for the incident, scattering, and total waves in all three regions. Using a MATLAB software package [35] homemade code for this paper's conditions was implemented. The obtained simulation results are presented and discussed in the next section.

Results and discussion

Figure 2 represents the relative intensity distribution at the x-y plane for TM polarized light incident on a core-shell porous silica cylinder with core diameter D=6 μm, and shell thicknesses d=0.5 μm. The formation of PNJ and the variation of its characteristics with the change of porosity is obvious from this figure. The scattered and incident wave interactions lead to the confinement of electromagnetic energy in the shadow side of the microcylinder. With increasing the porosity, the length of the PNJ and the focal length increase, but the relative energy decreases. The longer PNJs often have weak local confinement and poor peak intensity [36].

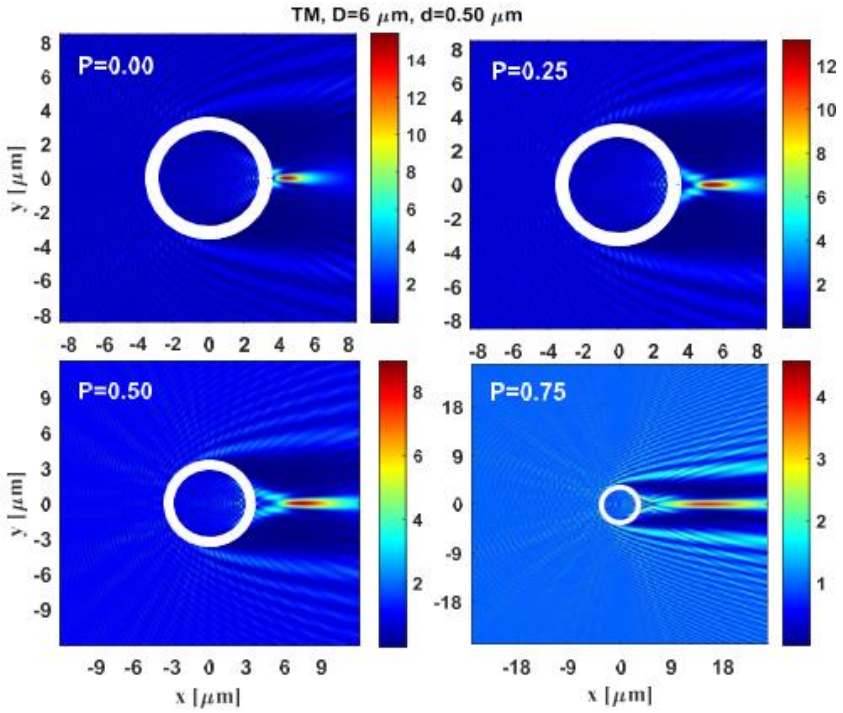

Fig 2. Relative intensity distribution at x-y plane for TM polarized light incidence (D=6 μm, d=0.5 μm)

The curves of relative intensity along the x-axis for TM polarized light incident are presented in Figure 3. The porosity has varied as a parameter in this figure. As shown in Figure 3, the intensities of the peaks decrease with increasing porosity, but the positions of the peaks are elongated. Maximum relative intensity achieved to 15.414 at focal length f= 0.963 μm, for fused silica case (P=0). With increasing porosity to P=0.75, relative intensity decreases to 4.071 and focal length increases to f= 11.550 μm. In the 0.75 porosity case, there are two focal points which we here restrict ourselves to the far focal spot. Because this one is more obvious than the near focal spot. Actually, by increasing porosity from 0 to 0.75 relative intensity reduces almost threefold, and focal length increases nearly twelve times. The elongated focal length of PNJ can be appropriate for near-field focusing applications such as size detection of a single nanoparticle [3,37].

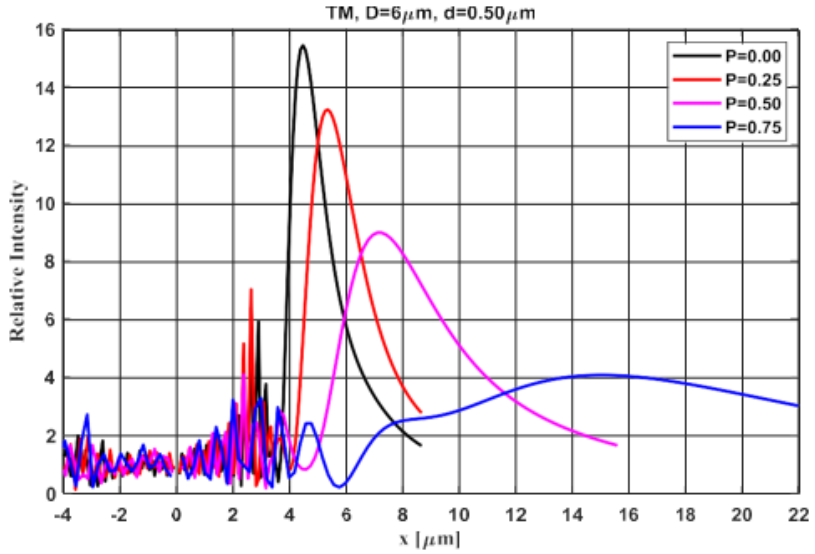

Fig 3. Relative intensity along the x-axis for TM polarized light incidence (D=6 μm, d=0.5 μm)

The transverse relative intensity distribution along the y-axis at the focal spot for various porosities is shown in Figure 4 at the TM polarized light incidence. The FWHM of photonic nanojet increases with increasing porosity. Subsequently, for porosity 0.00, 0.25, 0.50, and 0.75 the values of FWHM are 350.0, 437.5, 612.5, and 1225.0 nm, respectively. With increasing porosity, the effective refractive index of the porous core-shell microcylinder decreases according to Equation 3. As a result, the refractive index contrast between the microcylinder and its surrounding medium decreases. Therefore, the FWHM of PNJ increases with porosity.

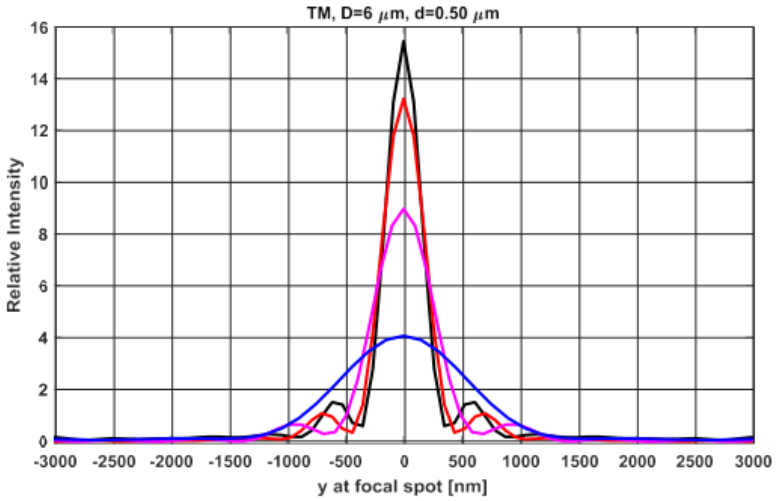

Fig 4. Relative intensity distribution along the y-axis at the focal spot for TM polarized light incidence (D=6 μm, d=0.50 μm)

Variations of the four main parameters of PNJ for various porosity and shell thicknesses are depicted in Figure 5. At fixed shell thicknesses focal length, length of PNJ, and FWHM are increased, and maximum relative intensity is decreased by increasing porosity. The largest focal length, 11.55 μm achieved for 0.50 μm shell thickness at 0.75 porosity. The longest PNJ (18.75 μm) is obtained for 0.75 μm shell thickness at 0.75 porosity. The narrowest PNJ is formed by the pure silica microcylinder with FWHM near 300 nm (almost equal to one-half of the incident wavelength). This finding agrees with the results of [38] for dielectric core-gold shell microcylinder and plane wave incidence on microsphere dielectric [20].

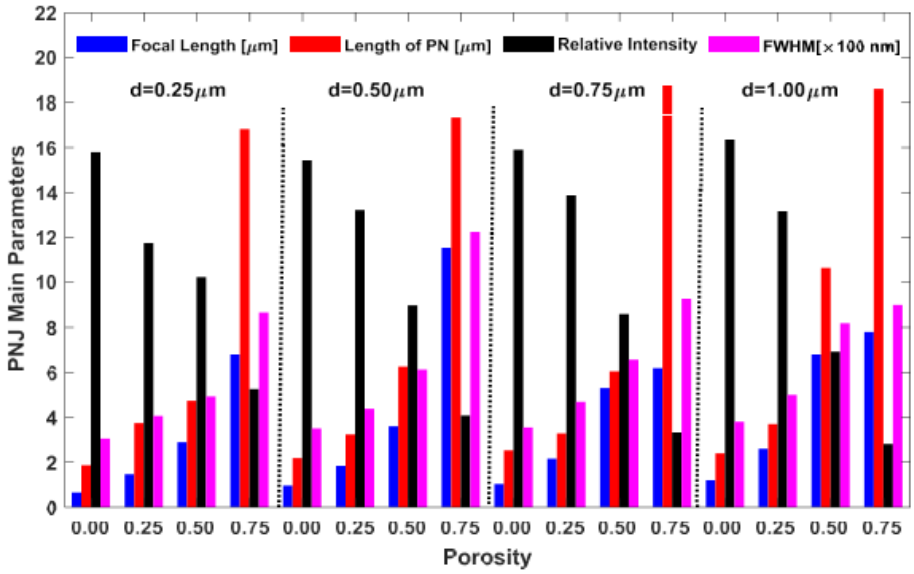

Fig 5. Main parameters of PNJ for TM polarized light incidence (D=6 μm)

The relative intensity distribution at the x-y plane for TE polarized light incidence is depicted in Figure 6. The peak intensity of PNJ decreases and the focal length of it is elongated with increasing porosity. The relative intensities of PNJ in Figure 5 are less than in Figure 2. As the refractive index contrast between the dielectric and surrounding medium in PNJ decreases, the maximum relative intensity at the focal spot decreases [36]. According to equations 3 and 4, the reduction of refractive index contrast between the porous core-shell microcylinder and its surrounding medium (air) for the TE case is less than for TM polarized light with increasing porosity.

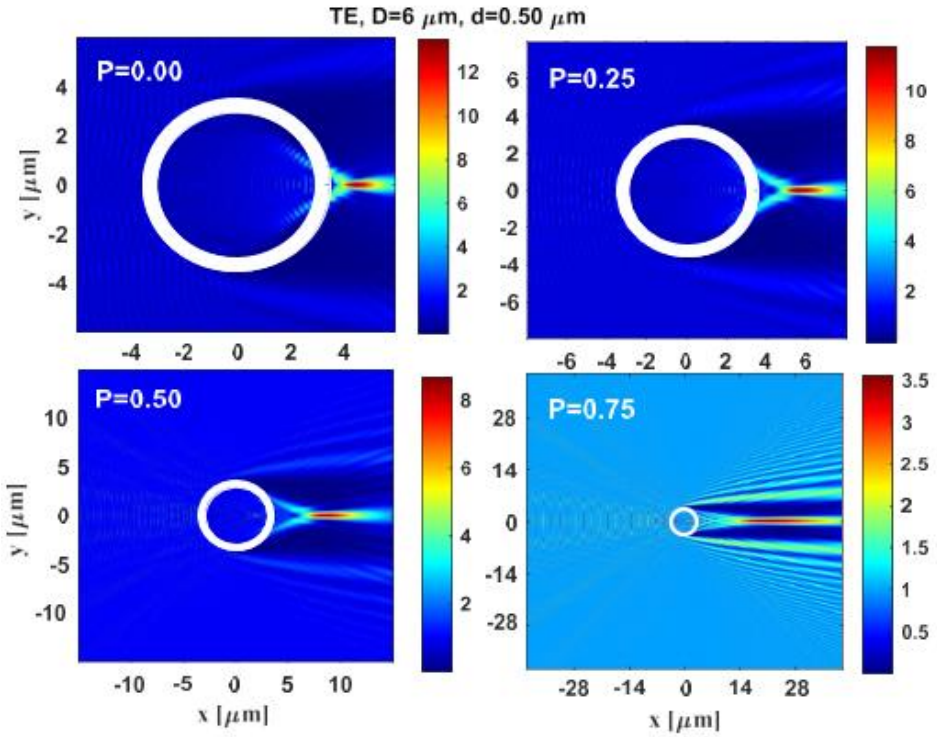

Fig 6. Relative intensity distribution at x-y plane for TE polarized light incidence (D=6 μm, d=0.5 μm)

A comparison of TE and TM polarizations for the main parameters of PNJ is depicted in Figure

7. Variations of PNJ focal length for TE and TM polarized light at various shell thicknesses and porosity are shown in Figure 7a. At fixed shell thicknesses, the focal length of PNJ is increased by increasing porosity for TM polarization mode. A great focal length increase is observed at

0.50 μm shell thicknesses and 0.75 porosity. In all shell thicknesses and porosity, the focal length for TE polarized light is larger or equal to TM mode except d= 0.50 μm and P=0.75 case. For TE polarization, at 0.25 μm shell thickness, the focal length of PNJ is regularly increased by increasing porosity. Meanwhile, at other shell thicknesses (0.5, 0.75, and 1.00 μm), the PNJ focal length is increased until P=0.50 and then is decreased for porosity 0.75.

The length of PNJ has a behavior that is the same as that of focal length, with one exception at porosity 0.75. So according to Figure 7b at porosity 0.75 and all shell thicknesses, the length of PNJ by TM polarization is larger than TE.

As shown in Figure 7c, at fixed shell thicknesses by increasing porosity, relative intensity is decreased for both TE and TM polarizations. Also, at a fixed porosity with increasing shell thicknesses, the relative intensity of PNJ at the focal point decreases. In all shell thicknesses and porosities, the maximum relative intensity at the focal spot for TE polarization is smaller than TM polarization. This behavior can be related to how the refractive index contrast between the

microcylinder and its surroundings area changes with porosity. By comparing Figures 2 and 5, the same result was obtained too.

As shown in Figure 7d, FWHM of formed PNJ by TE or TM polarized light is increased by increasing porosity at all shell thicknesses. At shell thickness 0.25 µm for pure silica microcylinder, the narrowest PNJ is achieved that FWHM of it is almost one-half of the incident wavelength. However, the relative intensity of PNJ is less in this situation, so, to reach higher intensities must be used porous silica cylinder. With tuning shell thicknesses and porosity of the core in the proposed PNJ structure can be obtained proper characteristic of PNJ for specific applications.

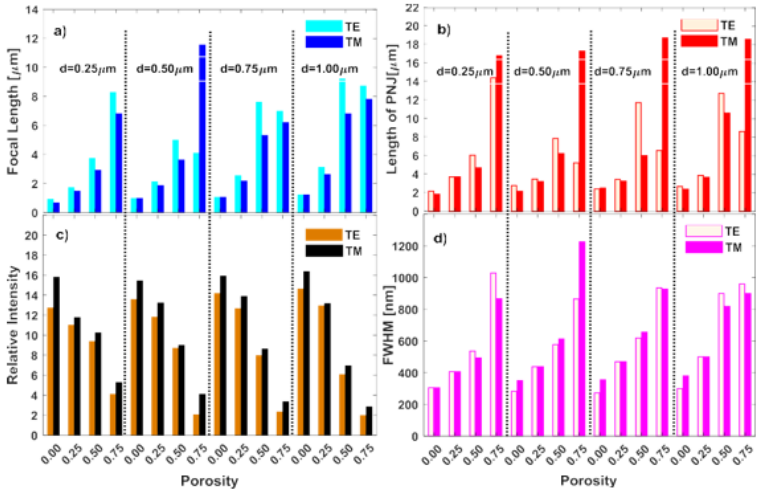

Fig 7. Comparing TE and TM polarizations a) Focal length, b) Length of PNJ, c) Relative Intensity, d) FWHM of PNJ (D=6 µm)

To investigate the core diameter effect on the main PNJ parameters, simulations were done for PNJ with a 5 µm core diameter. Figure 8 shows the relative intensity distribution of PNJ at the x- y plane by TM polarized light incidence in four different porosity and fixed 0.50 µm shell thicknesses. Change of porosity same as Figures 2 and 6 has an effective impact on the parameters of PNJ. Figure 8 shows that large focal length, elongated length of PNJ, and broader FWHM by low intensity are achieved for higher porosity.

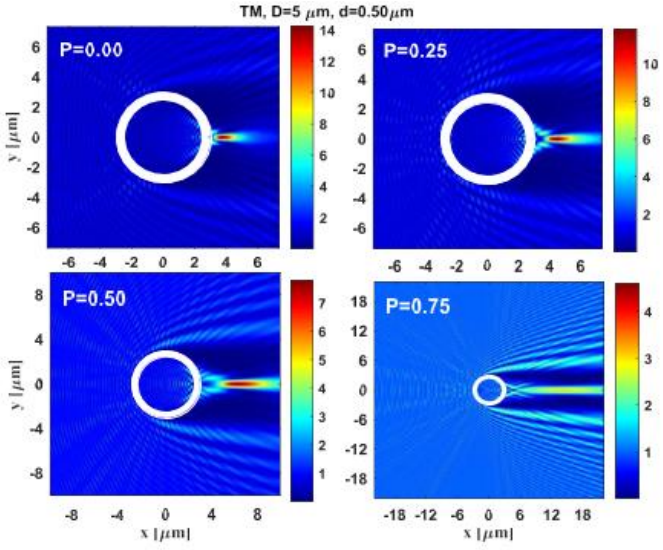

Fig 8. Relative intensity distribution at x-y plane for TM polarized light incidence (D=5 µm, d=0.5 µm)

Variations of the relative intensity along the x-axis for TM polarized light incident on a 5 µm diameter core – 0.50 µm shell thicknesses porous silica microcylinder is shown in Figure 9. The relative intensity of the peaks decreases with increasing porosity and the position of these peaks is further away from the shadow edge of the microcylinder. By comparison with Figure 3, it is obvious that with a 5 µm core diameter microcylinder the relative intensity enhancement is less than from a 6 µm diameter microcylinder. There are two focal points in the 0.75 porosity case. The far focal spot has a relative intensity more than the other.

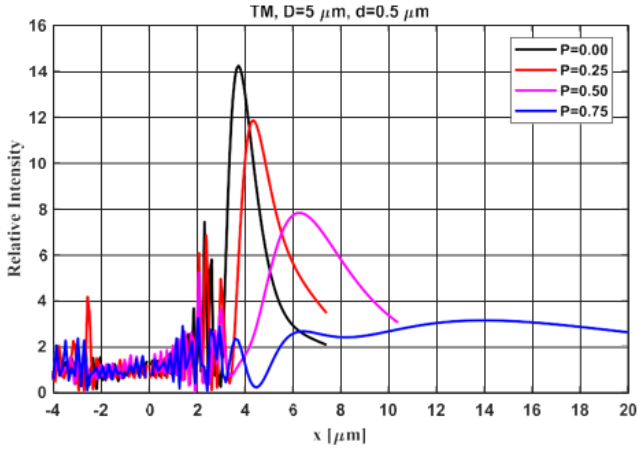

Fig 9. Relative intensity along the x-axis for TM polarized light incidence (D=5 µm, d=0.5 µm) A comparison of four main PNJ parameters for 5 and 6 µm diameter core-shell microcylinder is depicted in Figure 10. It is clear from Figure 10a that the focal length for the 6 µm diameter is slightly larger than the 5 µm diameter case at all porosities. According to Figure 10b, the length of PNJ formed by the microcylinder with core diameters of 5 and 6 µm is not much different. Figure 10c shows that the relative intensity at the focal point for 6 µm diameter PNJ is larger than 5 µm diameter at all porosity. FWHM is narrower for 5 µm diameter PNJ until 0.50 porosity, after this value of porosity both 5 and 6 µm diameter PNJs have the same beam waist (see Figure 10d). Therefore, the narrowest PNJ is achievable with small porosities and diameters of dielectric microcylinder.

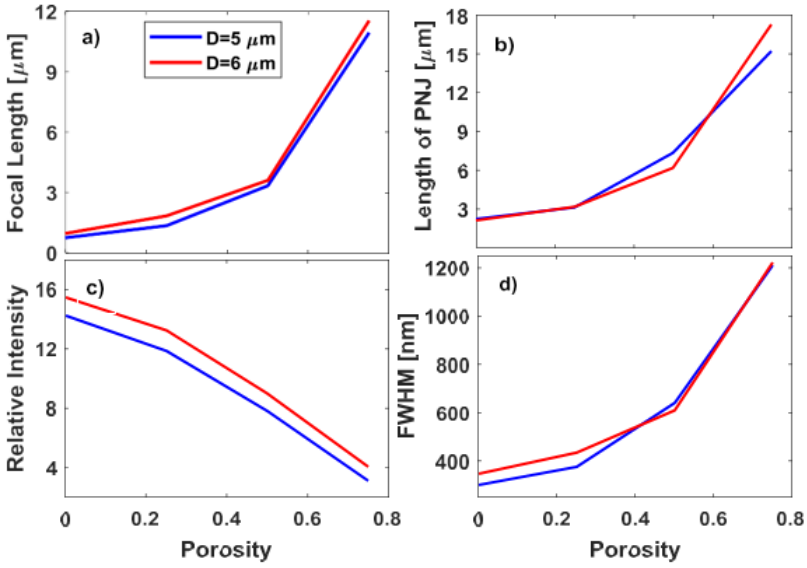

Fig 10. Four main PNJ parameters for 5 and 6 µm diameter a) Focal length, b) Length of PNJ, c) Relative intensity, d) FWHM at TM polarized incidence (d=0.50 µm)

Conclusion

A silica core-shell microcylinder photonic nanojet with cylindrical pores is theoretically investigated. The core of the microcylinder is formed from porous silica that is filled by air. The shell of the microcylinder is made of fused silica. The electromagnetic wave with TE or TM polarization normally radiates on the silica core-shell microcylinder. Four main PNJ parameters i.e., focal length, length of PNJ, relative intensity, and FWHM were studied. The boundary value method was employed to calculate the redistribution of electromagnetic wave intensity scattered from silica core-shell microcylinder. The porosity of cylinder pores, core diameter, shell thicknesses, and type of incident light polarization have a significant impact on the main parameters of photonic nanojet.

The simulation results show that with increasing the porosity, focal length, the PNJ length and FWHM are increased at fixed shell thicknesses. However, relative intensity at the focal point is decreased by increasing porosity. The focal length for TE polarized light is larger or equal to the TM polarization case in many structural conditions. Furthermore, core-shell microcylinders with large diameters have high relative intensity at the focal point. Also, the narrower PNJ is achieved with a small diameter and less porosity. The appropriate photonic nanojet for particular applications is accessible by tuning the geometrical (core diameter and shell thicknesses) and physical (porosity) parameters of the porous silica core-shell microcylinder.

References

1. Lecler S, Haacke S, Lecong N, Crégut O, Rehspringer J-L, Hirlimann C. Photonic jet driven non-linear optics: example of two-photon fluorescence enhancement by dielectric microspheres. Optics express. 2007; 15: 4935-4942.
2. Cui X, Erni D, Hafner C. Optical forces on metallic nanoparticles induced by a photonic nanojet. Optics express. 2008; 16: 13560-13568.
3. Gu G, Song J, Chen M, Peng X, Liang H, Qu J. Single nanoparticle detection using a photonic nanojet. Nanoscale. 2018; 10: 14182-14189.
4. Li H, Song W, Zhao Y, Cao Q, Wen A. *Optical trapping, sensing, and imaging by photonic nanojets*. In *Photonics*. 2021. MDPI.
5. Li Y, Xin H, Liu X, Zhang Y, Lei H, Li B. Trapping and detection of nanoparticles and cells using a parallel photonic nanojet array. ACS nano. 2016; 10: 5800-5808.
6. Yang H, Trouillon R, Huszka G, Gijs MA. Super-resolution imaging of a dielectric microsphere is governed by the waist of its photonic nanojet. Nano letters. 2016; 16: 4862-4870.
7. Darafsheh A. Photonic nanojets and their applications. Journal of Physics: Photonics. 2021; 3: 022001.
8. Jacassi A, Tantussi F, Dipalo M, Biagini C, Maccaferri N, Bozzola A, De Angelis F. Scanning probe photonic nanojet lithography. ACS applied materials & interfaces. 2017; 9: 32386-32393.
9. Chen W-Y, Liu Y-Y, Ngan Kong JA, Li LP-H, Chen Y-B, Cheng C-H, Liu C-Y. Biological cell trapping and manipulation of a photonic nanojet by a specific microcone-shaped optical fiber tip. Optics Letters. 2023; 48: 1216-1219.
10. Kovrov A, Novitsky A, Karabchevsky A, Shalin AS. A photonic nanojet as tunable and polarization- sensitive optical tweezers. Annalen der Physik. 2018; 530: 1800129.
11. Neves AAR. Photonic nanojets in optical tweezers. Journal of Quantitative Spectroscopy and Radiative Transfer. 2015; 162: 122-132.

12. Ferrand P, Wenger J, Devilez A, Pianta M, Stout B, Bonod Net al. Direct imaging of photonic nanojets. Optics express. 2008; 16: 6930-6940.
13. Kong S-C, Taflove A, Backman V. Quasi one-dimensional light beam generated by a graded-index microsphere. Optics Express. 2009; 17: 3722-3731.
14. Liu Y, Liu X, Li L, Chen W, Chen Y, Huang Y, Xie Z. Characteristics of photonic nanojets from two-layer dielectric hemisphere. Chinese Physics B. 2017; 26: 114201.
15. Soh JH, Wu M, Gu G, Chen L, Hong M. Temperature-controlled photonic nanojet via VO 2 coating. Applied Optics. 2016; 55: 3751-3756.
16. Wang Y-J, Dai C-A, Li J-H. Numerical study of tunable photonic nanojets generated by biocompatible hydrogel core-shell microspheres for surface-enhanced Raman scattering applications. Polymers. 2019; 11: 431.
17. Yang J, Twardowski P, Gérard P, Duo Y, Fontaine J, Lecler S. Ultra-narrow photonic nanojets through a glass cuboid embedded in a dielectric cylinder. Optics Express. 2018; 26: 3723-3731.
18. Yousefi M, Scharf T, Rossi M. Photonic nanojet generation under converging and diverging beams. JOSA B. 2021; 38: 317-326.
19. Li S, Xu J, Pang T, Yao H, Cheng H, Wang Jet al. Tailoring aberration-free photonic nanojets through the illumination of dielectric cylinders using cylindrical vector beams. Optics Letters. 2024; 49: 3682-3685.
20. Chen R, Lin J, Jin P, Cada M, Ma Y. Photonic nanojet beam shaping by illumination polarization engineering. Optics Communications. 2020; 456: 124593.
21. Uenohara T, Mizutani Y, Takaya Y. Comparison of intensity distribution of photonic nanojet according to Gaussian beam and radially polarization beam incidence. Precision Engineering. 2019; 60: 274-279.
22. Brandt J, Dittrich G, Thelen M, Renner H, Huber P, Eich M, Petrov A. On the applicability of the Maxwell Garnett effective medium model to media with a high density of cylindrical pores. Optical Materials Express. 2024; 14: 871-879.
23. Pacholski C. Photonic crystal sensors based on porous silicon. Sensors. 2013; 13: 4694-4713.
24. Davis ME. Ordered porous materials for emerging applications. Nature. 2002; 417: 813-821.
25. Moon JH, Kim S, Yi G-R, Lee Y-H, Yang S-M. Fabrication of ordered macroporous cylinders by colloidal templating in microcapillaries. Langmuir. 2004; 20: 2033-2035.
26. Velev O, Jede T, Lobo R, Lenhoff A. Porous silica via colloidal crystallization. Nature. 1997; 389: 447- 448.
27. Huang T-T, Rahmadiawan D, Shi S-C. Synthesis and characterization of porous silica and composite films for enhanced CO_2 adsorption: A circular economy approach. Journal of Materials Research and Technology. 2024; 32: 1460-1468.
28. Damadi MM, Kouhi M, Sobhanian S, Vahedi A, Maralani AA. Scattering and enhancement of electromagnetic waves energy by coaxial plasma cylinders. Journal of Quantitative Spectroscopy and Radiative Transfer. 2024; 313: 108831.
29. Zhang S, Zhang W, Liu L. Light scattering by a charged infinite cylinder in a transparent medium. Journal of Quantitative Spectroscopy and Radiative Transfer. 2020; 253: 107167.
30. Malitson IH. Interspecimen comparison of the refractive index of fused silica. Josa. 1965; 55: 1205- 1209.

31. Markel VA. Introduction to the Maxwell Garnett approximation: tutorial. JOSA A. 2016; 33: 1244- 1256.
32. Schmidt D, Schubert M. Anisotropic Bruggeman effective medium approaches for slanted columnar thin films. Journal of Applied Physics. 2013; 114:
33. Sareni B, Krähenbühl L, Beroual A, Brosseau C. Effective dielectric constant of random composite materials. Journal of Applied Physics. 1997; 81: 2375-2383.
34. Sihvola AH, *Electromagnetic mixing formulas and applications*. 1999: Iet.
35. Schäfer J. *MatScat*. 2016; Available from: http://www.mathworks.com/matlabcentral/fileexchange/36831.
36. Patel H, Majumder S. T. 1: Photonic nanojet: generation, manipu-lation and applications. 2018;
37. Yang Y-J, Zhang D-L, Xue S-D, Yuan N. Effective method for photonic jet shaping in reflection mode. Optics Express. 2024; 32: 26374-26385.
38. Liu C-Y. Superenhanced photonic nanojet by core-shell microcylinders. Physics Letters A. 2012; 376: 1856-1860.